

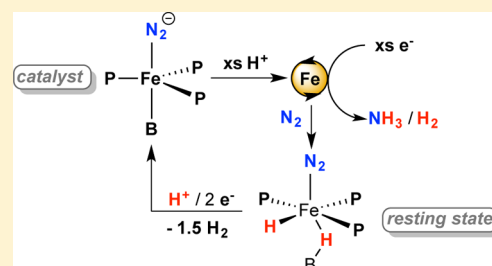
A Synthetic Single-Site Fe Nitrogenase: High Turnover, Freeze-Quench ^{57}Fe Mössbauer Data, and a Hydride Resting State

Trevor J. Del Castillo,[†] Niklas B. Thompson,[†] and Jonas C. Peters*

Division of Chemistry and Chemical Engineering, California Institute of Technology (Caltech), Pasadena, California 91125, United States

S Supporting Information

ABSTRACT: The mechanisms of the few known molecular nitrogen-fixing systems, including nitrogenase enzymes, are of much interest but are not fully understood. We recently reported that Fe–N₂ complexes of tetradentate P₃^E ligands (E = B, C) generate catalytic yields of NH₃ under an atmosphere of N₂ with acid and reductant at low temperatures. Here we show that these Fe catalysts are unexpectedly robust and retain activity after multiple reloadings. Nearly an order of magnitude improvement in yield of NH₃ for each Fe catalyst has been realized (up to 64 equiv of NH₃ produced per Fe for P₃^B and up to 47 equiv for P₃^C) by increasing acid/reductant loading with highly purified acid. Cyclic voltammetry shows the apparent onset of catalysis at the P₃^BFe–N₂/P₃^BFe–N₂[−] couple and controlled-potential electrolysis of P₃^BFe⁺ at −45 °C demonstrates that electrolytic N₂ reduction to NH₃ is feasible. Kinetic studies reveal first-order rate dependence on Fe catalyst concentration (P₃^B), consistent with a single-site catalyst model. An isostructural system (P₃^{Si}) is shown to be appreciably more selective for hydrogen evolution. In situ freeze-quench Mössbauer spectroscopy during turnover reveals an iron–borohydrido–hydride complex as a likely resting state of the P₃^BFe catalyst system. We postulate that hydrogen-evolving reaction activity may prevent iron hydride formation from poisoning the P₃^BFe system. This idea may be important to consider in the design of synthetic nitrogenases and may also have broader significance given that intermediate metal hydrides and hydrogen evolution may play a key role in biological nitrogen fixation.



1. INTRODUCTION

The fixation of molecular nitrogen (N₂) into ammonia (NH₃) is a transformation of fundamental importance to both biology and industry,¹ a fact which has prompted mechanistic study of the few known systems capable of catalyzing this reaction. The industrial Haber–Bosch process has been the subject of exhaustive investigation, resulting in a detailed mechanistic understanding in large part supported by surface spectroscopic studies on model systems.² The nitrogenase family of enzymes provides an example of catalytic N₂ conversion under ambient conditions and has also been studied extensively. While many questions remain unanswered regarding the mechanism of nitrogenase, a great deal of kinetic and reactivity information has been collected.³ Additionally, important insights have been provided by protein crystallography, X-ray emission spectroscopy, and site-directed mutagenesis studies, as well as in situ freeze-quench EPR and Mössbauer spectroscopy.^{4,5}

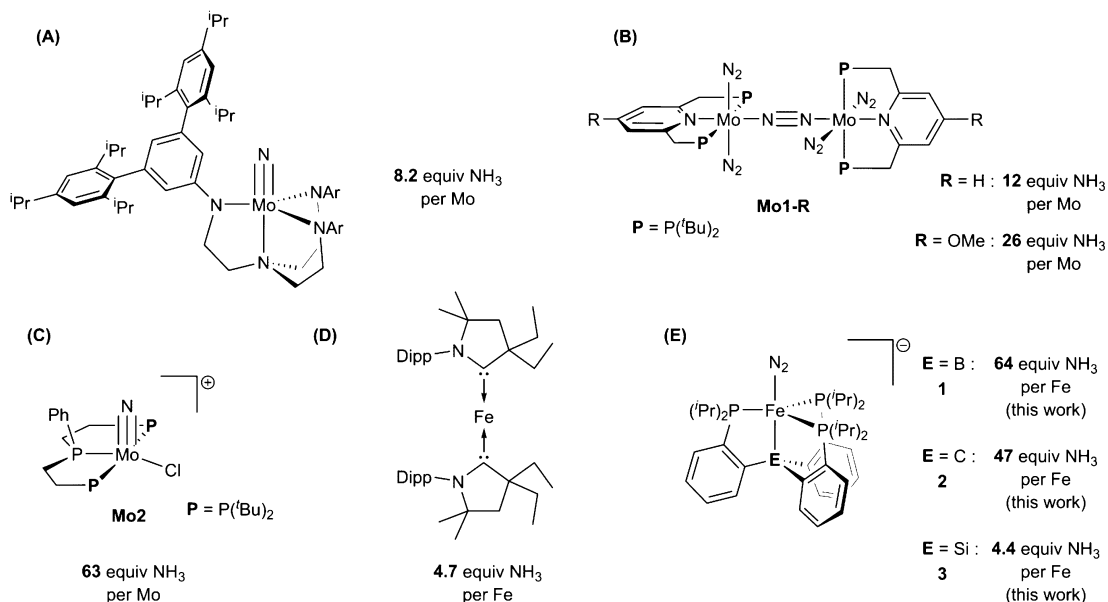
Hypotheses underpinning the mechanisms of both of these systems are bolstered by synthetic model chemistry and efforts to develop molecular N₂ conversion catalysts.⁶ This search has yielded systems capable of the catalytic reduction of N₂ to hydrazine (N₂H₄),⁷ tris(trimethylsilyl)amine,⁸ and a few examples of the direct catalytic fixation of N₂ to NH₃ (Chart 1).^{8g,9–12} While a wealth of mechanistic information for the original Mo catalyst system developed by Schrock has been derived from stoichiometric studies and theory,^{13,14} in situ spectroscopic studies during

catalysis were not reported. These synthetic catalysts operate under heterogeneous conditions and are likely to generate mixtures of intermediate species that are both diamagnetic and paramagnetic, making it challenging to reliably determine speciation under turnover. This latter limitation is also true of biological nitrogenases. While continuous-wave and pulsed EPR techniques can and have been elegantly applied,⁵ such studies are inherently limited in that species/intermediates not readily observable by these techniques will go unnoticed.

Iron is the only transition metal that is essential in the cofactor for nitrogenase function, and this fact has motivated a great deal of recent interest in Fe–N₂ model chemistry.¹⁵ In recent years we have focused on a family of Sacconi-type tetradentate ligands, P₃^E, in which three phosphine donors are bonded to a central atom through an *ortho*-phenylene linker (E = B, Si, C). We have shown that P₃^EM (M = Fe, Co) complexes promote the binding and activation of N₂, as well as the functionalization of bound N₂ with various electrophiles.^{16–18} Moreover, we discovered that P₃^BFe (P₃^B = tris(*o*-diisopropylphosphinophenyl)borane) and P₃^CFe (P₃^C = tris(*o*-diisopropylphosphinophenyl)methyl) complexes mediate the catalytic reduction of N₂ to NH₃ at low temperature using a strong acid, [H(OEt₂)₂][BAR^F₄] (HBAR^F₄ BAR^F₄ = tetrakis(3,5-bis(trifluoromethyl)phenyl)borate), and a

Received: February 16, 2016

Published: March 29, 2016

Chart 1. Synthetic Catalysts for Nitrogen Fixation with Maximum Observed Yields of NH₃^a

^a(A) See ref 9a. (B) See ref 10. (C) See ref 11. (D) See ref 8g. Dipp = 2,6-diisopropylphenyl. (E) See ref 12. Note that NH₃ equivalents shown represent the highest single-run values that have been reported for the various catalysts shown; direct cross-comparisons of Fe and Mo catalyst performance are tenuous due to the different reaction conditions used.

strong reductant, potassium graphite (KC₈) (Chart 1, E).¹² One unique aspect of these Fe-based systems is their suitability for in situ spectroscopic study by freeze-quench ⁵⁷Fe Mössbauer spectroscopy. In principle, this technique enables observation of the total Fe speciation as frozen snapshots during turnover.¹⁹ For single-site Fe nitrogenase mimics of the type we have developed, analysis of such data is far simpler than in a biological nitrogenase where many iron centers are present.²⁰

For the most active P₃^BFe catalyst system, many P₃^BFe–N₂H₂ model complexes that may be mechanistically relevant (e.g., Fe⁺, Fe–N₂[–], Fe=NNH₂⁺, Fe–NH₃⁺) have now been independently generated and characterized, including by ⁵⁷Fe Mössbauer spectroscopy, and these data facilitate interpretation of the freeze-quench Mössbauer data reported here. In combination with chemical quenching methods that we present to study the dynamics of product formation, it becomes possible to attempt to correlate the species observed spectroscopically with the N₂ fixing activity to gain a better understanding of the overall catalytic system. Such a strategy complements the studies of model complexes and stoichiometric reactions steps that we have previously undertaken and offers a fuller mechanistic picture. While many questions remain, this approach to studying N₂-to-NH₃ conversion mediated by synthetic iron catalysts is a mechanistically powerful one.

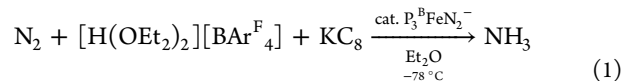
Here we undertake tandem spectroscopy/activity studies using the P₃^E (E = B, C, Si) Fe catalyst systems and report the following: (i) two of these Fe-based catalysts (E = B, C) are unexpectedly robust under the reaction conditions, demonstrating comparatively high yields of NH₃ that are nearly an order of magnitude larger than in initial reports at lower acid/reductant loadings; (ii) based on electrochemical measurements the dominant catalysis by the P₃^BFe system likely occurs at the formal P₃^BFe–N₂/P₃^BFe–N₂[–] couple, corroborated by demonstrating catalysis with Na/Hg and electrolytic N₂-to-NH₃ conversion in a controlled-potential bulk electrolysis; (iii) the P₃^BFe system shows first order rate dependence on iron catalyst concentration and zero order dependence on acid concentration;

(iv) kinetic competition between rates of N₂ versus H⁺ reduction are a key factor in determining whether productive N₂-to-NH₃ conversion is observed; and (v) a metal hydride–borohydride species is a resting state of the P₃^BFe catalysis system.

2. RESULTS AND DISCUSSION

2.1. Increased Turnover of Fe-Catalyzed N₂ Fixation and Evidence for Catalysis at the P₃^BFe–N₂/P₃^BFe–N₂[–] Couple.

Following our initial discovery that the addition of excess HBAR₄^F and KC₈ to the anionic dinitrogen complex [P₃^BFe(N₂)][(12-crown-4)₂Na] (1) at low temperature in Et₂O under an atmosphere of N₂ furnishes catalytic yields of NH₃, we pursued the optimization of this system for NH₃ yield (eq 1). Under our initially reported conditions (in Et₂O at



–78 °C with 48 equiv of HBAR₄^F and 58 equiv of KC₈) the catalysis furnishes 7.0 ± 1.0 equiv of NH₃ per Fe-atom, corresponding to 44% of added protons being delivered to N₂ to make NH₃. Initial attempts at optimization showed that neither the overall concentration of the reactants nor the mole ratio of the catalyst substantially altered the yield of NH₃ with respect to proton equivalents.

We have since examined whether the post-reaction material retained any catalytic competence when more substrate was delivered. We found that if, after stirring at –78 °C for 1 h the reaction mixture was frozen (at –196 °C), delivered additional substrate, and then thawed to –78 °C, significantly more NH₃ was formed. Iterating this reloading process several times resulted in a steady increase in the total yield of NH₃ per Fe-atom (Figure 1), demonstrating that some active catalyst remains at –78 °C, even after numerous turnovers. This result implies that the yield of NH₃ is limited by competitive consumption of substrate in a hydrogen-evolving reaction (HER).

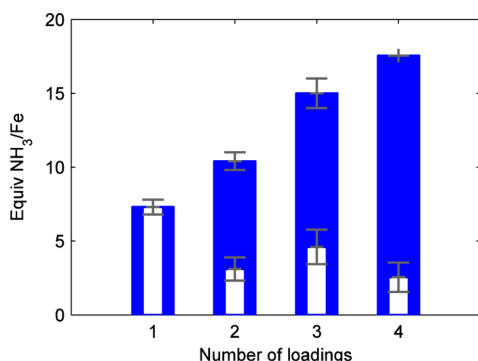


Figure 1. Yields of NH₃ obtained using P₃^BFe–N₂[−] **1** from successive reloading of HBAR₄^F and KC₈ to reactions maintained at ≤−70 °C in Et₂O. Blue bars denote total observed yields and white inset bars denote the average increase in total yield from the final loading of substrate. Each loading corresponds to 48 equiv of HBAR₄^F and 58 equiv of KC₈ relative to Fe. Data presented are averages of two experiments.

The apparent stability of at least some of the catalyst at low temperature suggested that it may be possible to observe higher turnover numbers if the catalyst is delivered more substrate at the beginning of the reaction. Indeed, as shown in Table 1, addition of increasing equivalents of HBAR₄^F and KC₈ to **1** at low temperature furnished steadily increasing yields of NH₃ relative to catalyst, with a current maximal observed yield of 64 equiv of NH₃ per Fe-atom (average of 59 ± 6 over 9 iterations, Table 1, entries 1–5) at 1500 equiv acid loading. This yield is nearly an order of magnitude larger than that reported at the original acid loading of 48 equiv. We note that the yields of NH₃ under these conditions are highly sensitive to the purity of the acid source, unsurprising given the high acid substrate loading relative to catalyst (1500 equiv of HBAR₄^F). To obtain reproducible yields, we have developed a tailored protocol for the synthesis of sufficiently pure NaBAR₄^F/HBAR₄^F, which is detailed in the Supporting Information. It is also important to ensure good

mixing and a high gas–liquid interfacial surface area to enable proper mass transfer in the heterogeneous reaction mixture.

Having discovered that P₃^BFe–N₂[−] **1** is a significantly more robust catalyst than originally appreciated, we investigated the activity of the alkyl N₂ anion [P₃^CFe–N₂][(Et₂O)_{0.5}K] (**2**) toward N₂ fixation at higher substrate loading. Significantly higher yields of NH₃ per Fe are also attainable using **2** as a catalyst, albeit with roughly 2/3 the activity of **1** (Table 1, entries 6–10). As a point of comparison, we also submitted the silyl congener [P₃^{Si}Fe–N₂][(12-crown-4)₂Na] (**3**) (P₃^{Si} = tris(*o*-diisopropylphosphinophenyl)silyl) to these conditions and observed dramatically lower yields of NH₃, consistent with earlier reports (Table 1, entries 11 and 12). Although the P₃^{Si}Fe–N₂[−] system **3** displays worse selectivity for NH₃ formation vs HER than **1** (*vide infra*), **3** still demonstrates catalytic yields of NH₃ under sufficiently high substrate loading (up to 4 equiv of NH₃ per Fe, Table 1, entry 12).

Table 1 also contains data for catalytic trials with the borohydrido–hydrido complex (P₃^B)(μ-H)Fe(H)(N₂) (**4-N₂**) as a catalyst in mixed Et₂O/toluene solvent. In the presence of admixed toluene **4-N₂** is observed to be partially soluble and demonstrates competence as a catalyst (Table 1, entry 14); in the absence of toluene **4-N₂** shows poor solubility and lower than catalytic yields of NH₃ were observed under the originally reported catalytic conditions (0.50 ± 0.1 equiv of NH₃ per Fe).^{12a} The significance of these observations is discussed below (section 2.4).

The efficiency of NH₃ production with respect to acid substrate decreases under increasingly high turnover conditions for these iron systems. Our understanding of the HER kinetics (*vide infra*) rationalizes this phenomenon in that under comparatively low catalyst loading (which engenders higher turnover) the background HER should be increasingly competitive, thereby reducing N₂-fixing efficiency. The product of the reaction (NH₃) may also act as an inhibitor of catalysis. To test this latter possibility, catalytic runs with 150 equiv of HBAR₄^F

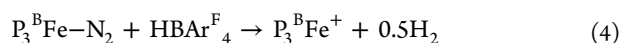
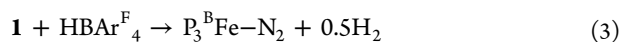
Table 1. NH₃ Generation from N₂ Mediated by Synthetic Fe Catalysts^a

N ₂ + [H(OEt ₂) ₂][BAR ₄ ^F] + KC ₈ $\xrightarrow[-78\text{ }^\circ\text{C}]{\text{catalyst, Et}_2\text{O}}$ NH ₃							
entry	catalyst	[Fe] (mM)	HBAR ₄ ^F (equiv)	KC ₈ (equiv)	variation	NH ₃ /Fe (equiv)	yield NH ₃ /H ⁺ (%)
1	1	1.3	48	58		7.3 ± 0.5	45 ± 3
2	1	0.64	96	58		12 ± 1	38 ± 3
3	1	0.43	150	185		17.4 ± 0.2	35.6 ± 0.4
4	1	0.08	720	860		43 ± 4	18 ± 2
5	1	0.04	1500	1800		59 ± 6	12 ± 1
6 ^b	2	1.0	37	40	[HBAR ₄ ^F] = 31 mM	4.6 ± 0.8	36 ± 6
7	2	0.56	110	120		11.3 ± 0.9	31 ± 2
8	2	0.28	220	230		14 ± 3	19 ± 4
9	2	0.08	750	810		19 ± 4	7 ± 2
10	2	0.04	1500	1600		36 ± 7	7 ± 1
11 ^c	3	0.58	48	58	[HBAR ₄ ^F] = 31 mM	0.8 ± 0.5	5 ± 3
12	3	0.04	1500	1800		3.8 ± 0.8	0.8 ± 0.2
13	4-N₂ ^d	–	150	185	3% toluene	1.1 ± 0.1	2.4 ± 0.3
14	4-N₂	0.44	150	185	25% toluene	5.6 ± 0.9	12 ± 2
15	1	0.41	150	185	25 equiv of NH ₃ added	6.4 ± 0.1	13.2 ± 0.2
16	1	0.41	150	0	1900 equiv of 10 wt% Na/Hg	5.0 ± 0.2	10.3 ± 0.5

^aFe precursor, HBAR₄^F, KC₈, and Et₂O sealed in a vessel at −196 °C under an N₂ atmosphere followed by warming to −78 °C and stirring at −78 °C. Unless noted otherwise, [HBAR₄^F] = 63 mM. Yields are reported as an average of at least 2 iterations; data for individual experimental iterations are presented in the Supporting Information. ^bData taken from ref 12b. ^cData taken from ref 12a. ^dNot fully soluble under reaction conditions.

and 185 equiv of KC_8 in the presence of **1** were conducted with the inclusion of 25 equiv of NH_3 (Table 1, entry 15). The fixed N_2 yield of this reaction is substantially lower than that of the comparable experiment without added NH_3 (Table 1, entry 3). One contributing cause for NH_3 inhibition is that it sequesters HBAr_4^{F} as $[\text{NH}_4][\text{BAr}_4^{\text{F}}]$; however, the yield of NH_3 observed in entry 15 is suppressed compared to an experiment with only 100 equiv of HBAr_4^{F} . This observation indicates that NH_3 inhibits the catalytic reaction, and that the degree of inhibition is more substantial than stoichiometric leveling of the acid strength.

We also sought to establish the minimum reducing potential required to drive catalysis with $\text{P}_3^{\text{B}}\text{Fe}-\text{N}_2^-$ **1**. We have shown in previous work that **1** reacts favorably with HBAr_4^{F} in Et_2O at -78°C along a productive N_2 fixation pathway.¹⁸ In brief, **1** can be doubly protonated in Et_2O at -78°C to generate $\text{P}_3^{\text{B}}\text{Fe}=\text{NNH}_2^+$ (eq 2). If only stoichiometric acid is present, **1** is instead unproductively oxidized to $\text{P}_3^{\text{B}}\text{Fe}-\text{N}_2$ (eq 3). We have only observed net oxidation in the reaction of the neutral $\text{P}_3^{\text{B}}\text{Fe}-\text{N}_2$ state with HBAr_4^{F} in Et_2O to produce $\text{P}_3^{\text{B}}\text{Fe}^+$ (eq 4).



These observations suggest that N_2 -fixing catalysis likely occurs at the $\text{P}_3^{\text{B}}\text{Fe}-\text{N}_2/\text{P}_3^{\text{B}}\text{Fe}-\text{N}_2^-$ redox couple (-2.2 V vs Fc/Fc^+), but not at the $\text{P}_3^{\text{B}}\text{Fe}^+/\text{P}_3^{\text{B}}\text{Fe}-\text{N}_2$ feature (-1.5 V vs Fc/Fc^+). We have explored this hypothesis via cyclic voltammetry (CV) experiments. Figure 2 shows electrochemical

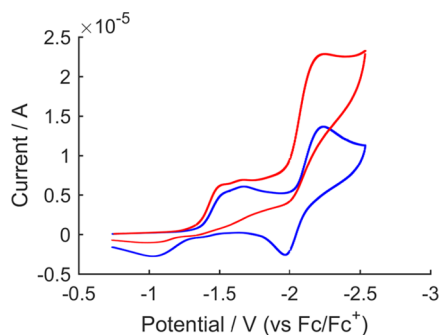


Figure 2. Cyclic voltammetry of $[\text{P}_3^{\text{B}}\text{Fe}][\text{BAr}_4^{\text{F}}]$ in the presence of 0 (blue trace) and 5 (red trace) equiv of HBAr_4^{F} , collected in Et_2O with 0.1 M $\text{NaBAr}_4^{\text{F}}$ electrolyte at -45°C using a glassy carbon electrode and referenced to the Fc/Fc^+ couple. Scan rate is 100 mV/s.

data for $\text{P}_3^{\text{B}}\text{Fe}^+$ dissolved in Et_2O at -45°C under 1 atm N_2 in the presence of 0.1 M $\text{NaBAr}_4^{\text{F}}$ as a soluble electrolyte to create a modestly conductive ethereal solution.²¹ The blue trace shows the expected irreversible $\text{P}_3^{\text{B}}\text{Fe}^+/\text{P}_3^{\text{B}}\text{Fe}-\text{N}_2$ feature centered around -1.5 V and the $\text{P}_3^{\text{B}}\text{Fe}-\text{N}_2/\text{P}_3^{\text{B}}\text{Fe}-\text{N}_2^-$ couple at -2.2 V , as previously reported.^{17a} The red trace shows the electrochemical behavior of $\text{P}_3^{\text{B}}\text{Fe}^+$ in the presence of 5 equiv of HBAr_4^{F} . The data reveal a sharp plateaued increase in current coincident with the $\text{P}_3^{\text{B}}\text{Fe}-\text{N}_2/\text{P}_3^{\text{B}}\text{Fe}-\text{N}_2^-$ redox couple, and very little increase in current at the $\text{P}_3^{\text{B}}\text{Fe}^+/\text{P}_3^{\text{B}}\text{Fe}-\text{N}_2$ feature. The onset of the rise in current at the $\text{P}_3^{\text{B}}\text{Fe}-\text{N}_2/\text{P}_3^{\text{B}}\text{Fe}-\text{N}_2^-$ couple intimates that electrocatalysis may be feasible, and that chemical reductants with weaker reduction potentials than KC_8 may also be competent for N_2 -to- NH_3 conversion catalyzed by $\text{P}_3^{\text{B}}\text{Fe}-\text{N}_2^-$.

Also, the potential at which the current increases does not shift from the $\text{P}_3^{\text{B}}\text{Fe}-\text{N}_2/\text{P}_3^{\text{B}}\text{Fe}-\text{N}_2^-$ couple in the absence of acid, indicating that this reduction precedes the first protonation event.

To determine whether electrolytic N_2 -to- NH_3 conversion contributes to the feature observed in the CV data,^{6c} a controlled-potential bulk electrolysis of $\text{P}_3^{\text{B}}\text{Fe}^+$ and 10 equiv of HBAr_4^{F} in Et_2O at -45°C under 1 atm N_2 in the presence of 0.1 M $\text{NaBAr}_4^{\text{F}}$ electrolyte with a reticulated vitreous carbon working electrode was performed. The electrolysis was held at -2.6 V (vs Fc/Fc^+) for 4.6 h, after which time 5.85 C of charge had been passed. Product analysis revealed the formation of NH_3 (18% faradaic efficiency) as well as H_2 (58% faradaic efficiency). The amount of NH_3 generated in this experiment corresponds to 0.5 equiv with respect to Fe and 14% yield with respect to acid. When the experiment was performed at higher acid loading (50 equiv), the NH_3 yield increased substantially (2.2 equiv per Fe; 25% faradaic efficiency; electrolysis held at -2.3 V in this instance with 8.39 C charge passed over 16.5 h). This electrolysis also produced 21.7 μmol of H_2 corresponding to 48% faradaic efficiency. While these yields of NH_3 with respect to Fe do not demonstrate formal turnover, they do suggest that electrocatalytic N_2 -to- NH_3 conversion by this iron system may be feasible. That the NH_3 yield increases with increased acid correlates well with our chemical activity results. Studies to more thoroughly explore the electrocatalytic N_2 -to- NH_3 conversion behavior of $\text{P}_3^{\text{B}}\text{Fe}$ species are underway.

The electrochemical data presented in Figure 2 also suggest that chemical reductants with weaker reduction potentials than KC_8 may be competent for N_2 -to- NH_3 conversion catalysis by **1**. Consistent with this notion, we find that catalytic yields of NH_3 (5 equiv per Fe) are obtainable using **1** in the presence of 150 equiv of HBAr_4^{F} and 1900 equiv of 10 wt% Na/Hg amalgam under $\sim 1\text{ atm}$ N_2 at -78°C in Et_2O (Table 1, entry 16; a larger excess of 10 wt% Na/Hg amalgam was employed to compensate for the lower surface area of the reagent). This result demonstrates that the catalysis is not unique to the presence of either potassium or graphite. KC_8 is a stronger reductant than is needed for N_2 -to- NH_3 conversion, but shows more favorable selectivity for N_2 reduction relative to H_2 generation than other reductants we have thus far canvassed.

2.2. Kinetics of Ammonia and Hydrogen Formation. To better understand the competing NH_3 - and H_2 -forming reactions that occur during catalysis, we measured the time profiles of product formation using the most active catalyst, $\text{P}_3^{\text{B}}\text{Fe}-\text{N}_2^-$ **1**. Our method for quenching catalytic NH_3 production uses rapid freeze-quenching of reactions to -196°C , followed by addition of *tert*-butyllithium ($t\text{BuLi}$), and subsequent annealing to -78°C . Employing this method allows for the measurement of NH_3 production as a function of time. The time courses of NH_3 formation obtained for the previously reported substrate loading (blue trace)^{12a} as well as a higher substrate loading (red trace) are shown in Figure 3.

Under both substrate loadings shown in Figure 3, the reaction proceeds to completion at -78°C . Furthermore, under the higher-turnover conditions (with 150 equiv of HBAr_4^{F} and 185 equiv of KC_8 , Figure 3, red triangles) the reaction proceeds to completion over $\sim 45\text{ min}$, a time scale that enables us to measure the dependence of $d[\text{NH}_3]/dt$ on the concentrations of the soluble reagents—**1** and HBAr_4^{F} —via the method of initial rates. As shown in Figure 4 (left), an initial rates analysis demonstrates that the reaction is first order in $[\text{Fe}]$, which is consistent with the involvement of a monomeric $\text{P}_3^{\text{B}}\text{Fe}$ species in the turnover-limiting step for NH_3 formation. Comparing conditions ranging from 15 mM to 250 mM $[\text{HBAr}_4^{\text{F}}]$ revealed no significant

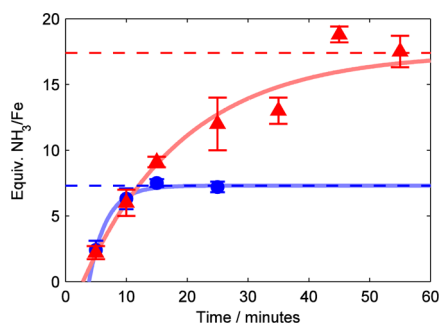


Figure 3. Time profiles of the formation of NH_3 from N_2 using **1** as a catalyst at -78°C under previously reported reaction conditions (blue circles, 0.64 mM **1**, 48 equiv of HBAr^{F_4} , 58 equiv of KC_8) and higher-turnover conditions (red triangles, 0.43 mM **1**, 150 equiv of HBAr^{F_4} , 185 equiv of KC_8). Dashed lines show expected final yields from the corresponding entries in Table 1 (entries 1 and 3). Each point represents an average of two experiments; data for the individual experimental iterations are presented in the Supporting Information. Solid lines are provided as guides for the eye only.

correlation between initial $[\text{HBAr}^{\text{F}_4}]$ and initial NH_3 production rate; for instance, there is no measurable difference in the amount of NH_3 produced after 5 min. This observation suggests zero-order rate dependence on acid concentration, which is borne out by the initial rates analysis (Figure 4, right).

These data provide an estimate of the initial turnover frequency (TOF, determined as moles of NH_3 produced per minute per Fe-atom) of this catalyst system of $1.2 \pm 0.1 \text{ min}^{-1}$. While the TOF of this catalyst is not directly comparable to other N_2 -to- NH_3 conversion catalysts due to differences in conditions and substrate, it is notable that **1** under the conditions used here furnishes a substantially higher TOF than the other synthetic systems in Chart 1 for which data is available (Table 2), despite operating over 100°C lower in temperature (albeit with the benefit of a stronger reductant). MoFe nitrogenase purified from *Klebsiella pneumoniae* exhibits a TOF of approximately 80 min^{-1} ,²² nearly 2 orders of magnitude faster than that of the present synthetic Fe system, while operating at room temperature.

To determine potential HER activity of $\text{P}_3^{\text{B}}\text{Fe}-\text{N}_2^-$ **1**, we measured the time course of $\text{H}_{2(\text{g})}$ formation from HBAr^{F_4} and KC_8 in the absence and presence of **1**, under catalytically relevant

Table 2. Comparison of NH_3 -Generating Reactions^b

catalyst	temp ($^\circ\text{C}$)	maximum yield ^c	TOF (min^{-1})	efficiency (%)
Mo1-H ^b	25	12	0.14	31
Mo2 ^c	25	63	0.26	35
1 ^d	-78	64	1.2	12

^aData for **Mo1-H** and **Mo2** are from ref 11 and depictions of the compounds are presented in Chart 1. ^bConditions: 2,6-lutidinium trifluoromethanesulfonate and cobaltocene in toluene. ^cConditions: 2,4,6-trimethylpyridinium trifluoromethanesulfonate and decamethylcobaltocene in toluene. ^dConditions: HBAr^{F_4} and KC_8 in diethyl ether. ^eExpressed in NH_3 equivalents.

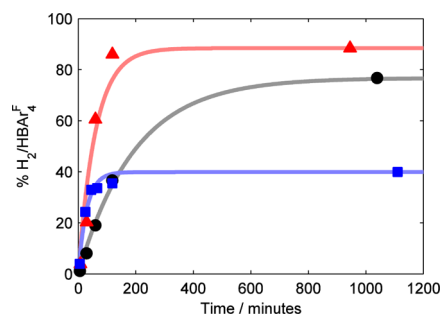


Figure 5. Time profiles of the formation of H_2 from HBAr^{F_4} and KC_8 in Et_2O at -78°C . Data is presented for the reaction of these reagents alone (black circles) as well as in the presence of **1** (blue squares) and **3** (red triangles). Each time course was collected continuously from a single experiment. Solid lines are provided as guides for the eye only.

conditions. As shown in Figure 5, the initial rate of $\text{H}_{2(\text{g})}$ evolution at -78°C is enhanced by the presence of **1**. The Fe-catalyzed HER is $>85\%$ complete within the first hour with a final yield of $\sim 40\%$ (blue trace).²³ Quantifying the NH_3 produced in this reaction (34% yield based on HBAr^{F_4}) accounts for 74% of the acid added. We also confirm that there is significant background HER from HBAr^{F_4} and KC_8 (black trace), as expected. We conclude that both catalyzed and background HER are competing with NH_3 formation in the catalyst system.

As a point of comparison, we also measured the rate of H_2 evolution in the presence of $\text{P}_3^{\text{Si}}\text{Fe}-\text{N}_2^-$ (**3**). As shown in Figure 5, **3** also catalyzes HER, with an initial rate that is

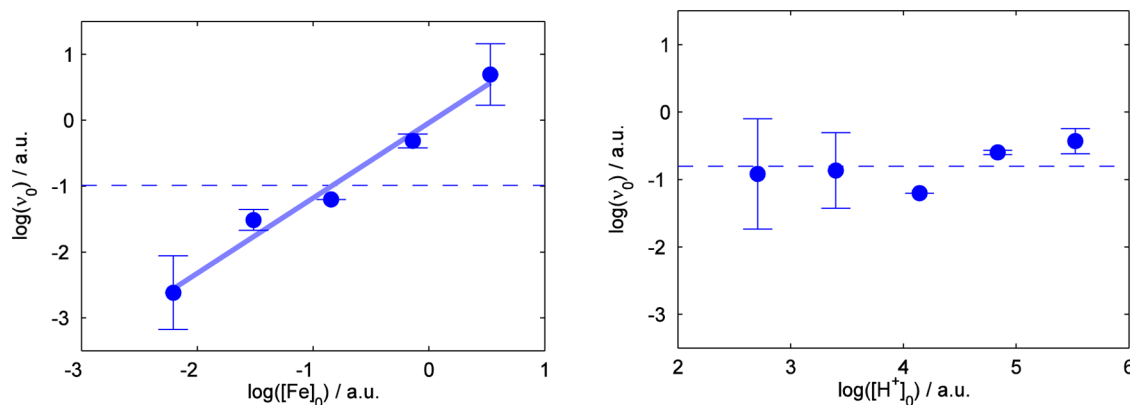


Figure 4. Log–log plots of the initial rate of NH_3 formation (ν_0) versus initial concentrations of soluble reagents. (Left) ν_0 versus $[\text{Fe}]_0$ for a range of **1** from 0.11–1.7 mM. The dashed line shows a constant function fit to the mean of the data, while the solid trend line shows the result of least-squares linear regression ($\log(\nu_0) = (-0.04 \pm 0.1) + (1.1 \pm 0.1) \cdot \log([\text{1}]_0)$, $r^2 = 0.98$). (Right) ν_0 versus $[\text{HBAr}^{\text{F}_4}]_0$ for a range of $[\text{HBAr}^{\text{F}_4}]$ from 15–250 mM. The dashed line shows a constant function fit to the mean of the data (RMSE = 0.3), which is not statistically different from the result of a least-squares linear regression (RMSE = 0.3). Data for individual experimental iterations and discussion of initial rates estimates are presented in the Supporting Information.

comparable to **1**. However, in this case, H₂ evolution approaches completion over 2 h, resulting in a final measured yield of 88%. This is consistent with the low N₂-fixing activity of **3**; in the absence of a competitive NH₃-producing reaction, **3** catalyzes the reduction of protons to H₂. Understanding the fundamental differences that give rise to the divergent selectivity of these Fe catalysts is an important goal in the context of designing selective N₂ reduction catalysts.

2.3. Spectroscopic Characterization of Fe Speciation under Turnover. Considering the relatively slow rate of NH₃ formation ascertained from low-temperature quenching experiments, we sought to determine the Fe speciation under turnover using the P₃^BFe–N₂[–] catalyst **1**. By rapidly freeze-quenching reaction mixtures using ⁵⁷Fe-enriched **1** as a catalyst, time-resolved Mössbauer spectra can be obtained reflective of catalysis.²⁴

The Mössbauer parameters of some independently synthesized P₃^BFe species that may be relevant to the present catalysis have been measured and are collected in Table 3. Mössbauer

Table 3. Mössbauer Parameters for P₃^BFe Complexes^a

compound	S	conditions	δ (mm s ⁻¹)	ΔE_Q (mm s ⁻¹)
P ₃ ^B Fe ⁺ ^b	3/2	frozen solution, 50 mT	0.75	2.55
P ₃ ^B Fe–N ₂ H ₄ ⁺	3/2	frozen solution, 50 mT	0.7	2.30
P ₃ ^B Fe–NH ₃ ⁺	3/2	frozen solution, zero field	0.68	1.94
P ₃ ^B Fe–NH ₂	3/2	frozen solution, zero field	0.60	1.47
P ₃ ^B Fe–N ₂ ^b	1	frozen solution, 50 mT	0.56	3.34
P ₃ ^B Fe–N ₂ ^{–b}	1/2	frozen solution, 50 mT	0.40	0.99
P ₃ ^B Fe–NNH ₂ ^{+b}	1/2	frozen solution, 50 mT	0.35	1.02
P ₃ ^B Fe–NAd ⁺	1/2	powder, 50 mT	0.15	1.31
(P ₃ ^B)(μ -H)Fe(H)(N ₂)	0	frozen solution, zero field	0.21	1.44
(P ₃ ^B)(μ -H)Fe(H)(H ₂)	0	frozen solution, zero field	0.19	1.55
P ₃ ^B Fe–NAd	0	powder, zero field	0.04	1.40

^aAll data were collected at 80 K under the conditions noted; external magnetic fields applied in parallel mode. ^bData taken from ref 18.

isomer shifts (δ) can often be used to assign the relative oxidation state of structurally related compounds,^{16b,25} yet in this series of P₃^BFe compounds there is a poor correlation between δ and formal oxidation state assignments (e.g., Fe–N₂[–] and Fe=NNH₂⁺ species have nearly identical isomer shifts). This fact reflects the high degree of covalency present in these P₃^BFe–N_xH_y complexes, skewing classical interpretations of the Mössbauer data; the degree of true oxidation/reduction at the iron centers in P₃^BFe–N_xH_y species is buffered by strong covalency with the surrounding ligand field.^{26,27} We do,

however, find a useful linear correlation ($r^2 = 0.90$) between the measured ground spin states (S) of P₃^BFe–N_xH_y compounds and δ (Figure 6),²⁸ providing an empirical relationship that guides analysis of Mössbauer spectra obtained from catalytic reactions. Ground spin states can be reliably correlated with the type of N_xH_y ligand, and possibly the presence of hydride ligands, coordinated to a P₃^BFe center. This knowledge, combined with freeze-quench Mössbauer data, enables us to predict with some confidence the type(s) of Fe species that are present in a spectrum obtained after freeze-quenching during turnover.

Figure 7 shows time-resolved Mössbauer spectra of freeze-quenched catalytic reaction mixtures of P₃^BFe–N₂[–] **1** with 48 equiv of HBAR₄^F and 58 equiv of KC₈. Figure 7A shows the spectrum of catalyst ⁵⁷Fe-**1** as a 0.64 mM solution in THF, which features a sharp, asymmetric quadrupole doublet at 80 K in the presence of a 50 mT external magnetic field. Figure 7B shows the spectrum of a catalytic reaction mixture freeze-quenched after 5 min of stirring, revealing the major Fe species (blue, representing ca. 60% of all Fe) present during active turnover to have parameters $\delta = 0.16 \pm 0.2$ mm s⁻¹ and $\Delta E_Q = 1.63 \pm 0.03$ mm s⁻¹, which, within the error of the simulation, is consistent with the diamagnetic borohydrido–hydrido species (P₃^B)(μ -H)Fe(H)(L) (**4-L**), where L = N₂ or H₂.²⁹ This observation correlates well with the previously reported result that **4-N₂** is produced from the reaction of **1** with smaller excesses of HBAR₄^F and KC₈.^{12a} Further corroborating this assignment, data collected at liquid He temperature with a small applied magnetic field suggest that this species is a non-Kramer's spin system,³⁰ and should be $S = 0$ given the observed correlation between δ and S (*vide supra*). Also present in Figure 7B is a minor component (~8%, shown in white) with parameters $\delta = 0.02 \pm 0.2$ mm s⁻¹ and $\Delta E_Q = 0.97 \pm 0.2$ mm s⁻¹, and a broad residual absorbance centered at $\delta \approx 0.9$ mm s⁻¹ encompassing a width of ~2 mm s⁻¹ (representing ca. 20–30% of all Fe in the sample, shown in gray). Due to the broadness of the latter resonance ($\Gamma \approx 1$ mm s⁻¹), this feature could not be accurately modeled. Nevertheless, the signal is consistent with several known $S = 3/2$ P₃^BFe species. For example, the vacant cation, P₃^BFe⁺, and the cationic species P₃^BFe–N₂H₄⁺ and P₃^BFe–NH₃⁺, are $S = 3/2$ species and give rise to quadrupole doublets that lie within the envelope of this broad signal (Table 3, entries 1–3).³¹ The utility of freeze-quench ⁵⁷Fe Mössbauer spectroscopy is evident; in a single spectral snapshot the presence of P₃^BFe-components with varied spin states including $S = 0, 1/2, 1,$ and $3/2$ are observed.

Figure 7C shows that the primary Fe species present after 25 min of reaction time is the starting catalyst **1** (shown in red,

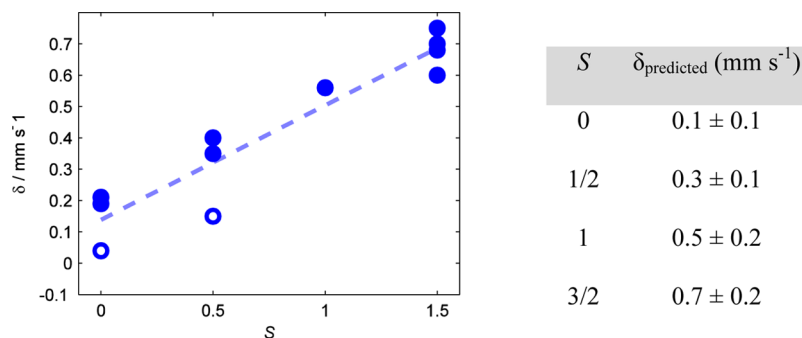


Figure 6. Plot of δ versus ground spin-state S for the compounds listed in Table 3 (blue circles), along with a linear least-squares fit to the data (dotted line, $r^2 = 0.90$). The isomer shifts of P₃^BFe–NAd^{0/+} are highlighted by open circles.²⁸ The table to the right lists the expectation values for δ based on S computed from the linear fit (ranges reported as 95% confidence interval).

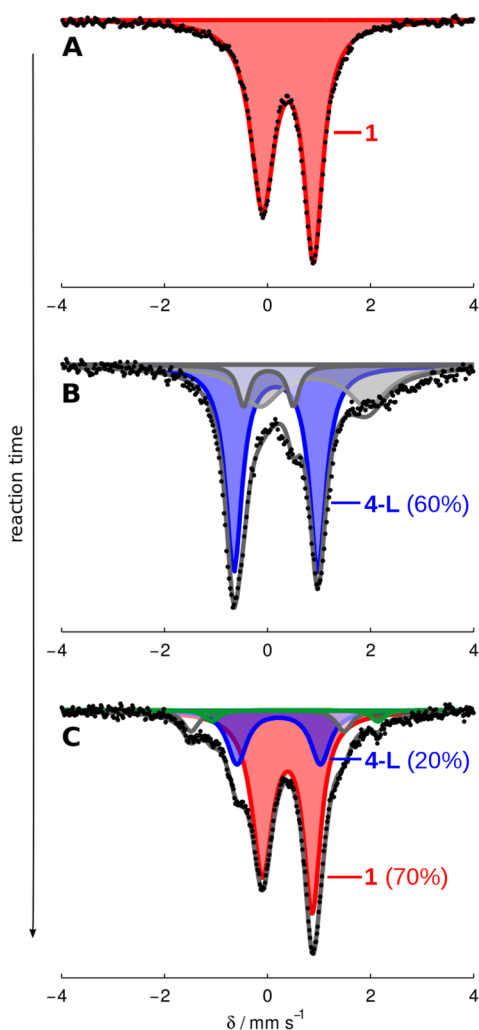


Figure 7. Frozen solution Mössbauer spectra collected at 80 K in the presence of a 50 mT parallel magnetic field. (A) Spectrum of **1** (0.64 mM in THF). (B) A catalytic mixture (Et_2O , 0.64 mM **1**, 48 equiv of HBAr^{F_4} , 58 equiv of KC_8) freeze-quenched after 5 min of stirring at -78°C . (C) A catalytic mixture (Et_2O , 0.64 mM **1**, 48 equiv of HBAr^{F_4} , 58 equiv of KC_8) freeze-quenched after 25 min of stirring at -78°C . Data are presented as black points and simulations as solid gray lines with components plotted as solid areas underneath the curve. For parameters of individual components see the SI.

representing ca. 70% of all Fe in the sample). Also present is ca. 20% of the species we assign as **4-L** ($\delta = 0.22 \pm 0.2 \text{ mm s}^{-1}$ and $\Delta E_{\text{Q}} = 1.62 \pm 0.03 \text{ mm s}^{-1}$, shown in blue), < 5% of the neutral dinitrogen complex, $\text{P}_3^{\text{B}}\text{Fe}-\text{N}_2$ (green), and ~7% of an as-yet unknown species with parameters $\delta = 0.00 \pm 0.02 \text{ mm s}^{-1}$ and $\Delta E_{\text{Q}} = 2.97 \pm 0.06 \text{ mm s}^{-1}$ (white). Thus, as acid substrate is consumed in the reaction to produce NH_3 and H_2 , the mixture of Fe species shown in Figure 7B at an early time point evolves back to the starting material **1**. A slight residual excess of KC_8 is needed to ensure recovery of the active catalyst. These data help rationalize the results of the substrate reloading experiments (*vide supra*).

The increasingly low Fe concentrations used to achieve the highest yields of NH_3 reported here make the collection of well-resolved Mössbauer spectra under such conditions challenging. Nonetheless, we repeated freeze-quench experiments for one set of higher-turnover conditions (Figure 8). Although in this case the Fe speciation at intermediate times appears more complex,

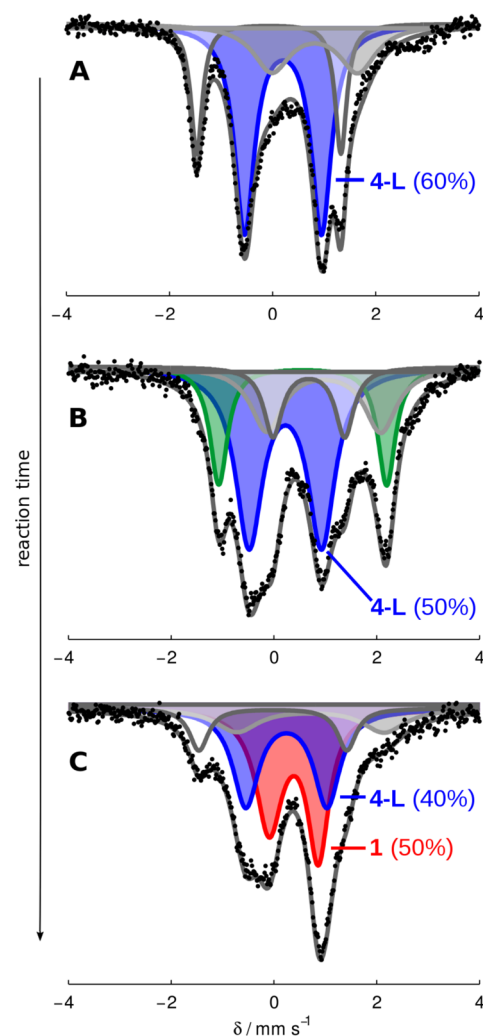


Figure 8. Frozen solution Mössbauer spectra collected at 80 K in the presence of a 50 mT parallel magnetic field. (A) A catalytic mixture (Et_2O , 0.43 mM **1**, 150 equiv of HBAr^{F_4} , 185 equiv of KC_8) freeze-quenched after 5 min of stirring at -78°C . (B) A catalytic mixture (Et_2O , 0.43 mM **1**, 150 equiv of HBAr^{F_4} , 185 equiv of KC_8) freeze-quenched after 10 min of stirring at -78°C . (C) A catalytic mixture (Et_2O , 0.43 mM **1**, 150 equiv of HBAr^{F_4} , 185 equiv of KC_8) freeze-quenched after 25 min of stirring at -78°C . Data presented as black points, simulations as solid gray lines with components plotted as solid areas underneath the curve. For parameters of individual components, see SI.

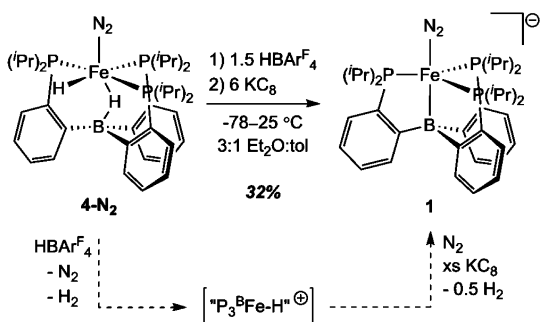
these data exhibit the same gross behavior shown in Figure 7; under active turnover the major Fe species present is consistent with hydride **4-L** ($\geq 50\%$, average parameters $\delta = 0.20 \pm 0.2 \text{ mm s}^{-1}$ and $\Delta E_{\text{Q}} = 1.49 \pm 0.09 \text{ mm s}^{-1}$, Figure 8A,B³²), and as the extent of reaction increases significant amounts of $\text{P}_3^{\text{B}}\text{Fe}-\text{N}_2^-$ reform (Figure 8C³³).

2.4. Precatalyst Activity of $(\text{P}_3^{\text{B}})(\mu\text{-H})\text{Fe}(\text{H})(\text{N}_2)$ (4-N₂**) and Identification of a Catalyst Resting State.** The observations presented in section 2.3 suggest that hydride **4-L** builds up as the major Fe-containing species during active turnover and appears to be converted back to the active catalyst **1** when catalysis is complete. We previously observed that this species can form under conditions that model the catalytic conditions (10 equiv of acid/12 equiv of reductant) and our initial thinking that **4-N₂** may be a catalyst deactivation product was guided by the poor activity of isolated **4-N₂** as a precatalyst

under the standard conditions (generating only 0.5 ± 0.1 equiv of NH_3 per Fe at 50 equiv of acid/60 equiv of reductant).^{12a} However, in that initial report we also noted that isolated 4-N_2 is not solubilized under the catalytic conditions. Therefore, in light of the current in situ spectroscopy, and the observation that 4-N_2 liberated some NH_3 under the original conditions, we wondered whether its insolubility may be responsible for its comparatively low activity as an isolated precursor. If 4-N_2 is brought into solution, or formed in solution during turnover, it may exhibit activity. To test this hypothesis we explored the activity of 4-N_2 under modified catalytic conditions where a toluene/ Et_2O mixture (which improves the solubility of 4-N_2) was employed as the solvent. In this case we find that 4-N_2 serves as a viable precatalyst (Table 1, entries 13 and 14). We suppose then that under the standard conditions (in pure Et_2O), if 4-L is generated in solution during catalysis, it should be able to react productively so long as it does not irreversibly precipitate, which may be slow at -78°C . Accordingly, we have observed that the Mössbauer spectrum of a sample taken from a standard catalytic mixture as described in section 2.3 can be filtered at low temperature and still displays substantial 4-L .

These results suggest the feasibility of the stoichiometric transformation of hydride 4-L into N_2 anion **1** under catalytically relevant conditions. In a previous report, we showed that 4-N_2 is stable for short periods to either HBAr^{F}_4 or KC_8 in Et_2O at room temperature, again noting its insolubility under these conditions.^{12a} Given the results above, we have reinvestigated this reactivity in Et_2O /toluene mixtures. Thus, the reaction of 4-N_2 with 1 equiv of HBAr^{F}_4 in 6:1 d_8 -toluene: Et_2O results in consumption of the starting material along with the appearance of several new, paramagnetically shifted ^1H NMR resonances. We hypothesize that protonolysis of either the terminal or bridging hydride moieties in 4-N_2 produces a cationic " $\text{P}_3^{\text{B}}\text{Fe}-\text{H}^+$ " species, which may then be reduced to liberate 0.5 equiv of H_2 and re-enter the catalytic manifold of $\{\text{P}_3^{\text{B}}\text{Fe}-\text{N}_2\}^{\text{n}}$ species under an N_2 atmosphere. Indeed, the sequential addition of 1.5 equiv of HBAr^{F}_4 followed by 6 equiv of KC_8 to 4-N_2 at -78°C in 3:1 Et_2O :toluene produces substantial amounts of **1** (32% yield, unoptimized; Scheme 1). This stoichiometric

Scheme 1. Stoichiometric Conversion of 4-N_2 into **1** under Catalytically Relevant Conditions^a



^aA proposed reaction pathway is shown along the dashed arrows. " $\text{P}_3^{\text{B}}\text{Fe}-\text{H}^+$ " is a plausible intermediate of this conversion but has not been thoroughly characterized.

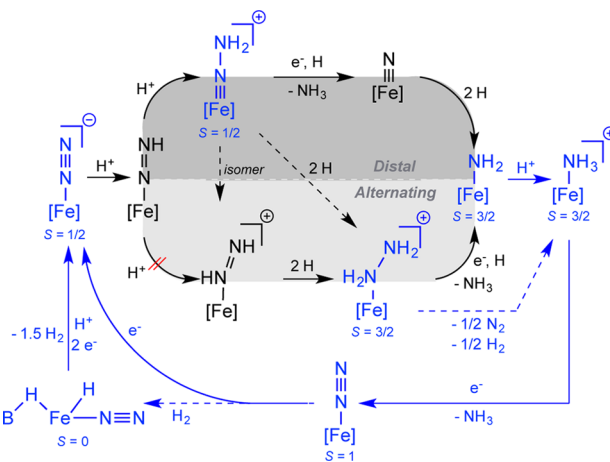
reactivity provides support for the idea that as 4-L is formed under the standard reaction conditions it can react with acid and reductant to produce the starting catalyst **1**, consistent with the observations provided in section 2.3.

Given that (i) 4-L appears to be the predominant Fe-containing species observed by freeze-quench Mössbauer spectroscopy under turnover conditions at early time points, (ii) this species serves as a competent precatalyst when solubilized, and (iii) 4-N_2 can be synthetically converted to **1** by HBAr^{F}_4 and KC_8 , we conclude that 4-L is a major resting state of the catalysis. This conclusion does not require 4-L to be an "on-path" intermediate; we instead think 4-L is more likely a resting state that ties up the catalyst, but one that reversibly leaks into the on-path catalytic cycle in which **1** is ultimately protonated.

The observation of a hydride resting state for this synthetic Fe catalyst may have additional relevance in the context of biological nitrogen fixation, where the intermediacy of metal hydride species has been proposed on the basis of spectroscopic data obtained during turnover.⁵ It has further been proposed that the reductive elimination of hydrides as H_2 may be a requisite component of N_2 binding to the nitrogenase active-site cofactor,^{22,34,35} giving rise to obligate H_2 evolution in the limiting stoichiometry of N_2 conversion to NH_3 .³⁶ The results described here directly implicate the relevance of a synthetic iron hydride species to a system capable of catalytic N_2 -to- NH_3 conversion. This in turn motivates complementary model reactivity studies on iron hydride species such as 4-L , targets whose relevance might otherwise be overlooked.

2.5. Summary of Mechanistically Relevant Observations. To help collect the information presented here and in related studies of the $\text{P}_3^{\text{B}}\text{Fe}$ -system, Scheme 2 provides a

Scheme 2. Possible Catalytic Scenarios for N_2 -to- NH_3 Conversion by **1**^a



^a[Fe] = $\text{P}_3^{\text{B}}\text{Fe}$. Thoroughly characterized species and their respective ground spin states S are shown in blue, while as-yet undetected species are shown in black. Blue arrows indicate known pathways that are likely kinetically competent (solid) at -78°C . Dashed arrows are likely incompetent pathways at -78°C .

mechanistic outline for the key iron species and plausible transformations we think are most relevant to the catalytic N_2 -to- NH_3 conversion cycle catalyzed by $\text{P}_3^{\text{B}}\text{FeN}_2^-$. The complexes shown in blue, along with their respective spin states S , have been thoroughly characterized. Also, the net conversions between complexes that are indicated by solid blue arrows have been experimentally demonstrated. Those complexes depicted in black have not (as yet) been experimentally detected.

Several results are worth underscoring. (i) We have characterized the $S = 3/2$, substrate-free state $\text{P}_3^{\text{B}}\text{Fe}^+$, and

shown that it binds N_2 upon electron loading, generating $S = 1$ $P_3^BFe-N_2$ or $S = 1/2$ $P_3^BFe-N_2^-$ depending on reducing equivalents provided.^{12a,17} $P_3^BFe^+$ is competent for catalytic N_2 -to- NH_3 conversion,^{12a} and facilitates this conversion electrocatalytically as established herein. (ii) The most reduced state, $P_3^BFe-N_2^-$ **1**, can be doubly protonated at low temperature to generate $P_3^BFe=NNH_2^+$, a distal pathway intermediate.¹⁸ This $S = 1/2$ species features a short Fe–N multiple bond (~ 1.65 Å). Its diamagnetic relative, $P_3^{Si}Fe=NNH_2^+$, has very recently been structurally characterized.³⁷ (iii) The $P_3^BFe=NNH_2^+$ intermediate anneals (in the absence of reductant) to generate significant amounts of $P_3^BFe-NH_3^+$.^{12a,18} (iv) $P_3^BFe-NH_3^+$ can also be generated by protonation of $P_3^BFe-NH_2$, and reductive displacement of NH_3 from $P_3^BFe-NH_3^+$ under N_2 regenerates $P_3^BFe-N_2^-$.^{17c}

Also worth emphasizing is that diamagnetic $P_3^{Si}Fe=NNH_2^+$ can be reduced at low temperature to $S = 1/2$ $P_3^{Si}Fe=NNH_2$, and this species (in the presence of acid/reductant equivalents) decays to a mixture of $P_3^{Si}Fe-N_2H_4^+$ and $P_3^{Si}Fe-NH_3^+$.³⁷ $P_3^{Si}Fe-N_2H_4^+$, and also $P_3^BFe-N_2H_4^+$, readily disproportionate the bound N_2H_4 to generate the corresponding NH_3 adducts $P_3^{Si}Fe-NH_3^+$ and $P_3^BFe-NH_3^+$,^{12a,16b} each of which evolves NH_3 upon reduction to regenerate (under N_2) $P_3^BFe-N_2^-$ **1** and $P_3^{Si}Fe-N_2^-$, respectively. The reaction pathway observed for $P_3^{Si}Fe=NNH_2^+$, more readily studied than for $P_3^BFe=NNH_2^+$ because $P_3^{Si}Fe=NNH_2^+$ can be isolated in pure form, highlights the possibility of a hybrid crossover mechanistic pathway wherein a distal intermediate (Fe=NNH₂) traverses to an alternating intermediate (Fe–N₂H₄) that may then be converted to NH_3 , possibly via disproportionation.^{18,37}

By demonstrating first-order rate dependence on the concentration of $P_3^BFe-N_2^-$, [**1**], the present study remains consistent with our hypothesis that a single-site mechanism is likely operative during N_2 -to- NH_3 conversion catalysis. The direct observation of both **1** and its neutral form $P_3^BFe-N_2$ in catalytic mixtures by freeze-quench Mössbauer spectroscopy lends further credence to this idea.

A plausible pathway for the formation of the putative resting state species **4-L** would be hydrogenation of $P_3^BFeN_2$ by evolved H_2 side product during catalysis. This process has been demonstrated independently at room temperature in benzene.²⁹ Follow-up control experiments in Et_2O , however, suggest that this reaction is not kinetically competent at -78 °C. We are therefore as present unsure of the dominant pathway by which **4-L** is formed during catalysis. Alternative pathways might include bimolecular H-atom transfers from as-yet unobserved intermediates with reactive N–H bonds, such as $P_3^BFe-N_2H$ and/or $P_3^BFe=NNH_2$.

3. CONCLUSION

In the present study we have shown that N_2 -fixing catalyst systems with P_3^EFe ($E = B, C, Si$) species give rise to high yields of NH_3 if supplied with sufficient acid and reductant. These yields (for $E = B$ and C) compare very favorably to the most active known Mo catalysts and are almost an order of magnitude greater than the yields presented in our previous reports. While we do not rule out some degree of catalyst degradation at -78 °C, these iron catalysts are unexpectedly robust and it is possible that the lower efficiency of catalysis at higher turnover is in part due to buildup of NH_3 product, which is an inhibitor. We have also provided new mechanistic insights for reactions with catalyst $P_3^BFe-N_2^-$ **1**, such as the observation that catalysis proceeds at -78 °C, the demonstration of first-order rate

dependence on catalyst concentration, the demonstration of zeroth-order rate dependence on $HBAr^F_4$ concentration, and the observation that **1** catalyzes HER as well as NH_3 formation. Preliminary electrochemistry data suggests that reductive chemistry mediated by the P_3^BFe system can be driven at the formal $P_3^BFe-N_2/P_3^BFe-N_2^-$ couple around -2.2 V vs Fc/Fc^+ , consistent with Na/Hg also serving as a viable reductant for catalytic turnover. Cyclic voltammetry and controlled potential electrolysis of $P_3^BFe^+$ at -45 °C demonstrate that electrolytic N_2 reduction is possible.

The present study has also demonstrated the utility of coupling in situ freeze-quench ^{57}Fe Mössbauer spectroscopy with kinetic analysis of product formation as a powerful tool for the mechanistic study of Fe-catalyzed N_2 fixation. To date, no synthetic molecular N_2 -to- NH_3 conversion catalyst system had been studied spectroscopically under active turnover conditions. Our freeze-quench Mössbauer results suggest that **4-L** is a resting state of the overall catalysis; this hydride species, which we previously posited to be primarily a catalyst sink, can instead reenter the catalytic pathway via its conversion to catalytically active $P_3^BFe-N_2^-$ **1**. This observation underscores the importance of understanding metal hydride reactivity in the context of Fe-mediated nitrogen fixation. It may be that HER activity provides a viable strategy for recovering catalytically active states from the unavoidable generation of iron hydride intermediates.

■ ASSOCIATED CONTENT

Supporting Information

The Supporting Information is available free of charge on the ACS Publications website at DOI: 10.1021/jacs.6b01706.

Experimental procedures and characterization data (PDF)

■ AUTHOR INFORMATION

Corresponding Author

*jpeters@caltech.edu

Author Contributions

†T.J.D.C. and N.B.T. contributed equally to this work.

Notes

The authors declare no competing financial interest.

■ ACKNOWLEDGMENTS

This work was supported by the NIH (GM 070757) and the Gordon and Betty Moore Foundation. T.J.D.C. acknowledges the support of the NSF for a Graduate Fellowship (GRFP), and N.B.T. acknowledges the support of the Resnick Sustainability Institute at Caltech for a Graduate Fellowship.

■ REFERENCES

- (1) Smil, V. *Enriching the Earth*; MIT Press: Cambridge, MA, 2001.
- (2) (a) Ertl, G. *J. Vac. Sci. Technol., A* **1983**, *1*, 1247. (b) Ertl, G. *Angew. Chem., Int. Ed.* **2008**, *47*, 3524.
- (3) Burgess, B. K.; Lowe, D. J. *Chem. Rev.* **1996**, *96*, 2983.
- (4) (a) Howard, J. B.; Rees, D. C. *Chem. Rev.* **1996**, *96*, 2965. (b) Einsle, O.; Tezcan, F. A.; Andrade, S. L. A.; Schmid, B.; Yoshida, M.; Howard, J. B.; Rees, D. C. *Science* **2002**, *297*, 1696. (c) Spatzal, T.; Aksoyoglu, M.; Zhang, L.; Andrade, S. L. A.; Schleicher, E.; Weber, S.; Rees, D. C.; Einsle, O. *Science* **2011**, *334*, 940. (d) Kowalska, J.; DeBeer, S. *Biochim. Biophys. Acta, Mol. Cell Res.* **2015**, *1853*, 1406.
- (5) Hoffman, B. M.; Lukoyanov, D.; Yang, Z.-Y.; Dean, D. R.; Seefeldt, L. C. *Chem. Rev.* **2014**, *114*, 4041.
- (6) (a) Chatt, J.; Leigh, G. J. *Chem. Soc. Rev.* **1972**, *1*, 121. (b) Khoenkhoen, N.; de Bruin, B.; Reek, J. N. H.; Dzik, W. I. *Eur. J.*

- Inorg. Chem.* **2015**, *4*, 567. (c) Pickett, C. J.; Talarmin, J. *Nature* **1985**, *317*, 652.
- (7) Bazhenova, T. A.; Shilov, A. E. *Coord. Chem. Rev.* **1995**, *144*, 69.
- (8) (a) Shiina, K. *J. Am. Chem. Soc.* **1972**, *94*, 9266. (b) Komori, K.; Oshita, H.; Mizobe, Y.; Hidai, M. *J. Am. Chem. Soc.* **1989**, *111*, 1939. (c) Tanaka, H.; Sasada, A.; Kouno, T.; Yuki, M.; Miyake, Y.; Nakanishi, H.; Nishibayashi, Y.; Yoshizawa, K. *J. Am. Chem. Soc.* **2011**, *133*, 3498. (d) Yuki, M.; Tanaka, H.; Sasaki, K.; Miyake, Y.; Yoshizawa, K.; Nishibayashi, Y. *Nat. Commun.* **2012**, *3*, 1254. (e) Ogawa, T.; Kajita, Y.; Wasada-Tsutsui, Y.; Wasada, H.; Masuda, H. *Inorg. Chem.* **2013**, *52*, 182. (f) Liao, Q.; Saffon-Merceron, N.; Mézailles, N. *Angew. Chem., Int. Ed.* **2014**, *53*, 14206. (g) Ung, G.; Peters, J. C. *Angew. Chem., Int. Ed.* **2015**, *54*, 532. (h) Siedschlag, R. B.; Bernales, V.; Vogiatzis, K. D.; Planas, N.; Clouston, L. J.; Bill, E.; Gagliardi, L.; Lu, C. C. *J. Am. Chem. Soc.* **2015**, *137*, 4638.
- (9) (a) Yandulov, D. V.; Schrock, R. R. *Science* **2003**, *301*, 76. (b) Ritleng, V.; Yandulov, D. M.; Weare, W. W.; Schrock, R. R.; Hock, A. S.; Davis, W. M. *J. Am. Chem. Soc.* **2004**, *126*, 6150.
- (10) (a) Arashiba, K.; Miyake, Y.; Nishibayashi, Y. *Nat. Chem.* **2011**, *3*, 120. (b) Tanka, H.; Arashiba, K.; Kuriyama, S.; Sasada, A.; Nakajima, K.; Yoshizawa, K.; Nishibayashi, K. *Nat. Commun.* **2014**, *5*, 3737. (c) Kuriyama, S.; Arashiba, K.; Nakajima, K.; Tanaka, H.; Kamaru, N.; Yoshizawa, K.; Nishibayashi, Y. *J. Am. Chem. Soc.* **2014**, *136*, 9719.
- (11) Arashiba, K.; Kinoshita, E.; Kuriyama, S.; Eizawa, A.; Nakajima, K.; Tanaka, H.; Yoshizawa, K.; Nishibayashi, Y. *J. Am. Chem. Soc.* **2015**, *137*, 5666.
- (12) (a) Anderson, J. S.; Rittle, J.; Peters, J. C. *Nature* **2013**, *501*, 84. (b) Creutz, S.; Peters, J. C. *J. Am. Chem. Soc.* **2014**, *136*, 1105. (c) Del Castillo, T. J.; Thompson, N. B.; Suess, D. L. M.; Ung, G.; Peters, J. C. *Inorg. Chem.* **2015**, *54*, 9256.
- (13) Schrock, R. R. *Angew. Chem., Int. Ed.* **2008**, *47*, 5512.
- (14) For theoretical work regarding the (PNP)Mo system developed by Nishibayashi, see refs 10b,c and the following: Tian, Y.-H.; Pierpont, A. W.; Batista, E. R. *Inorg. Chem.* **2014**, *53*, 4177.
- (15) See, for example: (a) McWilliams, S. F.; Holland, P. L. *Acc. Chem. Res.* **2015**, *48*, 2059–2065. (b) Field, L. D.; Li, H. L.; Dalgarno, S. J.; Turner, P. *Chem. Commun.* **2008**, 1680–1682. (c) Crossland, J. L.; Tyler, D. R. *Coord. Chem. Rev.* **2010**, *254*, 1883–1894. (d) Peters, J. C.; Mehn, M. P. *Bio-Organometallic Approaches to Nitrogen Fixation. In Activation of Small Molecules*; Tolman, W. B., Ed.; Wiley-VCH: Weinheim, Germany, 2006; p 81. (e) Hendrich, M. P.; Gunderson, W.; Behan, R. K.; Green, M. T.; Mehn, M. P.; Betley, T. A.; Lu, C. C.; Peters, J. C. *Proc. Natl. Acad. Sci. U. S. A.* **2006**, *103*, 17107–17112. (f) Grubel, K.; Brennessel, W. W.; Mercado, B. Q.; Holland, P. L. *J. Am. Chem. Soc.* **2014**, *136*, 16807.
- (16) (a) Mankad, N. P.; Whited, M. T.; Peters, J. C. *Angew. Chem., Int. Ed.* **2007**, *46*, 5768. (b) Lee, Y.; Mankad, N. P.; Peters, J. C. *Nat. Chem.* **2010**, *2*, 558.
- (17) (a) Moret, M.-E.; Peters, J. C. *Angew. Chem., Int. Ed.* **2011**, *50*, 2063. (b) Moret, M.-E.; Peters, J. C. *J. Am. Chem. Soc.* **2011**, *133*, 18118. (c) Anderson, J. S.; Moret, M.-E.; Peters, J. C. *J. Am. Chem. Soc.* **2013**, *135*, 534.
- (18) Anderson, J. S.; Cutsail, G., III; Rittle, J.; Connor, B.; Gunderson, W.; Zhang, L.; Hoffman, B.; Peters, J. C. *J. Am. Chem. Soc.* **2015**, *137*, 7803.
- (19) (a) Krebs, C.; Price, J. C.; Baldwin, J.; Saleh, L.; Green, M. T.; Bollinger, J. M. *Inorg. Chem.* **2005**, *44*, 742. (b) Krebs, C.; Bollinger, J. M. *Photosynth. Res.* **2009**, *102*, 295.
- (20) (a) McLean, P. A.; Papaefthymiou, V.; Orme-Johnson, W. H.; Münck, E. *J. Biol. Chem.* **1987**, *262*, 12900. (b) Yoo, S. J.; Angove, H. C.; Papaefthymiou, V.; Burgess, B. K.; Münck, E. *J. Am. Chem. Soc.* **2000**, *122*, 4926.
- (21) Data were not collected at -78 °C due to lower solubility of $\text{NaBAr}^{\text{F}}_4$ at that temperature.
- (22) Lowe, D. J.; Thorneley, R. N. F. *Biochem. J.* **1984**, *224*, 877.
- (23) This represents a lower limit of the H_2 produced due to leakage using a setup that enables quantification of H_2 and NH_3 in a single experiment.
- (24) (a) Daifuku, S. L.; Al-Afyouni, M. H.; Snyder, B. E. R.; Kneebone, J. L.; Neidig, M. L. *J. Am. Chem. Soc.* **2014**, *136*, 9132. (b) Daifuku, S. L.; Kneebone, J. L.; Snyder, B. E. R.; Neidig, M. L. *J. Am. Chem. Soc.* **2015**, *137*, 11432.
- (25) Berry, J. F.; Bill, E.; Bothe, E.; DeBeer, S.; Mienert, B.; Neese, F.; Wieghardt, K. *Science* **2006**, *312*, 1937.
- (26) Lee, Y.; Peters, J. C. *J. Am. Chem. Soc.* **2011**, *133*, 4438.
- (27) Ye, S.; Bill, E.; Neese, F. *Inorg. Chem.* **2016**, *55*, 3468.
- (28) If the adamantyl imide species $\text{P}_3^{\text{B}}\text{Fe}-\text{NAd}^{0/1+}$ are excluded from the series of data collected in Figure 6, the correlation improves significantly ($r^2 = 0.96$). The isomer shifts of these imides appear to be systematically reduced by ca. 0.1–0.2 mm s^{-1} from the trend exhibited by the rest of the compounds in Table 3.
- (29) Fong, H.; Moret, M.-E.; Lee, Y.; Peters, J. C. *Organometallics* **2013**, *32*, 3053.
- (30) Münck, E. *Methods Enzymol.* **1978**, *54*, 346.
- (31) Although the low isomer shift of the minor component present in Figure 7B is suggestive of a diamagnetic ground state, its identity is presently unknown.
- (32) Also present in Figure 8A: ca. 20% of the species with parameters $\delta = -0.03 \pm 0.04 \text{ mm s}^{-1}$ and $\Delta E_{\text{Q}} = 2.88 \pm 0.09 \text{ mm s}^{-1}$ that is present in Figure 7C (white), and ca. 20% of a broad residual signal consistent with an unresolved quartet species (gray). Also present in Figure 8B: ca. 20% of neutral $\text{P}_3^{\text{B}}\text{Fe}-\text{N}_2$ (green); ca. 15% of a sharply resolved species with parameters $\delta = 0.68 \text{ mm s}^{-1}$ and $\Delta E_{\text{Q}} = 1.40 \text{ mm s}^{-1}$ (white) that is consistent with a quartet species such as $\text{P}_3^{\text{B}}\text{Fe}-\text{NH}_2$; ca. 20% of a broad residual signal consistent with an unresolved quartet species (gray).
- (33) Also present in Figure 8C: ca. 10% of the species with parameters $\delta = -0.03 \pm 0.04 \text{ mm s}^{-1}$ and $\Delta E_{\text{Q}} = 2.88 \pm 0.09 \text{ mm s}^{-1}$ that is present in Figures 7C and 8A (white), and ca. 15% of a broad residual signal consistent with an unresolved quartet species (gray).
- (34) (a) Thorneley, R. N. F.; Lowe, D. J. *Biochem. J.* **1984**, *224*, 887. (a1) Lowe, D. J.; Thorneley, R. N. F. *Biochem. J.* **1984**, *224*, 895. (a2) Thorneley, R. N. F.; Lowe, D. J. *Biochem. J.* **1984**, *224*, 903. (35) Lukoyanov, D.; Yang, Z.-Y.; Khadka, N.; Dean, D. R.; Seefeldt, L. C.; Hoffman, B. M. *J. Am. Chem. Soc.* **2015**, *137*, 3610.
- (36) (a) Rivera-Ortiz, J. M.; Burris, R. H. *J. Bacteriol.* **1975**, *123*, 537. (b) Simpson, F. B.; Burris, R. H. *Science* **1984**, *224*, 1095.
- (37) Rittle, J.; Peters, J. C. *J. Am. Chem. Soc.* **2016**, *138*, 4243.